ChemMedChem

ResearchArticle
doi.org/10.1002/cmdc.202200139

Chemistry Europe
European Chemical Societies Publishing

www.chemmedchem.org

VIP *Very Important Paper*

Special Collection

Adsorption to the Surface of Hemozoin Crystals: Structure-Based Design and Synthesis of Amino-Phenoxazine β-Hematin Inhibitors

Tania Olivier,[a] Leigh Loots,[a] Michélle Kok,[b] Marianne de Villiers,[b] Janette Reader,[c] Lyn-Marié Birkholtz,[c] Gareth E. Arnott,[a] and Katherine A. de Villiers*[a]

In silico adsorption of eight antimalarials that inhibit β-hematin (synthetic hemozoin) formation identified a primary binding site on the (001) face, which accommodates inhibitors *via* formation of predominantly π-π interactions. A good correlation ($r^2 = 0.64$, $P = 0.017$) between adsorption energies and the logarithm of β-hematin inhibitory activity was found for this face. Of 53 monocyclic, bicyclic and tricyclic scaffolds, the latter yielded the most favorable adsorption energies. Five new amino-phenoxazine compounds were pursued as β-hematin inhibitors based on adsorption behaviour. The 2-substituted phenoxazines show good to moderate β-hematin inhibitory activity (< 100 μM) and *Plasmodium falciparum* blood stage activity against the 3D7 strain. N^1,N^1-diethyl-N^4-(10*H*-phenoxazin-2-yl)pentane-1,4-diamine (**P2a**) is the most promising hit with IC_{50} values of 4.7 ± 0.6 and 0.64 ± 0.05 μM, respectively. Adsorption energies are predictive of β-hematin inhibitory activity, and thus the *in silico* approach is a beneficial tool for structure-based development of new non-quinoline inhibitors.

Introduction

While significant strides have been made towards eliminating malaria in a number of countries, the disease is not under control.[1] On the contrary; statistics released by the World Health Organization suggest that progress has stalled, and the COVID-19 pandemic has only exacerbated this further.[2] The global number of cases increased from 227 million in 2019 to 241 million in 2020, with the African region accounting for the majority of the increased incidence. Treatment of the disease using artemisinin combination therapies (ACTs) forms an integral part of the current action plan; however, this is threatened by parasite resistance to artemisinin, which has already been established in the Greater Mekong subregion in Southeast Asia and detected more recently in the WHO African region. Thus, the development of new treatments remains an important endeavour. In this regard, the ferriprotoporphyrin IX detoxification pathway is an attractive drug target since it is crucial to the survival of the intraerythrocytic malaria parasite.[3] The end product, crystalline hemozoin (HZ), is a biomarker of infection by numerous blood-feeding organisms including the malaria parasite.[4] The mechanisms of crystal nucleation and growth have been the focus of numerous studies; several authors have proposed the involvement of various proteins,[5] while convincing evidence to the contrary supports the mediation of synthetic hemozoin (β-hematin) formation by lipids in the absence of proteins.[6] The aqueous-lipid interface has been shown to be important in facilitating crystal nucleation and growth.[6a,7] In particular, the neutral lipid 1-monomyristoyl glycerol been shown to orientate β-hematin crystals with their molecularly-flat (100) faces relative to the interface.[8] Using soft X-ray tomography imaging, Kapishnikov *et al.* have recently confirmed this orientation of HZ crystals relative to the inner membrane of the digestive vacuole (DV).[9]

The development of a heme fractionation assay has provided key insights regarding the cellular mode of action of hemozoin-inhibiting antimalarial drugs, of which examples include chloroquine (CQ) and amodiaquine (AQ).[10] Concomitant with a decrease in HZ formation, Combrinck *et al.* have shown that inhibitors of this class induce an increase in cellular free heme, and may ultimately form parasiticidal complexes with the latter.[11] It has been proposed that HZ inhibitors act *first* via adsorption to the crystal surface, thereby causing the observed dose-dependent increase in free heme as adsorption sites (for further crystal growth) are blocked by inhibitors.[12] This hypothesis underpins a kinetic model that is able to

[a] Dr. T. Olivier, Dr. L. Loots, Prof. G. E. Arnott, Dr. K. A. de Villiers
Department of Chemistry and Polymer Science,
Stellenbosch University
Private BagX1, Matieland 7602 (South Africa)
E-mail: kdev@sun.ac.za
[b] M. Kok, Dr. M. de Villiers
Department of Biochemistry,
Stellenbosch University
Private BagX1, Matieland, 7602 (South Africa)
[c] Dr. J. Reader, Prof. L.-M. Birkholtz
Department of Biochemistry, Genetics and Microbiology,
Institute for Sustainable Malaria Control,
University of Pretoria, Pretoria 0028 (South Africa)

Supporting information for this article is available on the WWW under https://doi.org/10.1002/cmdc.202200139

This article belongs to the Joint Special Collection "Biological and Medicinal Chemistry in Africa".

account for an observed decrease in rate constant for the formation of β-hematin in the presence of both quinoline and non-quinoline inhibitors.[13] Notably, a significant correlation was found between β-hematin inhibitory activity (IC_{50} values) and equilibrium adsorption constants (K_{ads}) extracted from fits to the kinetic model.[14]

Given that adsorption of inhibitors to the surface of the hemozoin/β-hematin crystal has a cascade effect on the survival of the parasite, this crucial step affords a valuable drug target. Solomonov *et al.* showed that crystals of β-hematin grown in methanol-DMSO or chloroform solutions containing CQ or quinine (QN) displayed tapered ends, and suggested that adsorption of these drugs to the (001) and (011) faces could account for this visual change in morphology.[15] Changes in the intensities of marker bands in the Raman spectrum of β-hematin samples grown in the presence of inhibitors provide further support for the adsorption of quinoline drugs to the crystal surface.[16] Similarly, investigations in saturated citric acid/n-octanol using atomic force microscopy point to the ability of CQ and related antimalarial drugs to adsorb onto the molecularly-flat (100) face between advancing islands.[17] The authors propose that CQ, QN and pyronaridine (PYR) act *via* a step-pinning mechanism, while AQ and mefloquine (MQ) preferentially adsorb to three-dimensional kinks.[18] The adsorption of inhibitors to the crystal surface has also been probed previously using *in silico* approaches. Two decades ago, Leiserowitz and co-workers undertook a theoretical morphology study of HZ and proposed a mechanism of drug action *via* direct adsorption.[19] The (001) face was found to have the most negative attachment energy of the expressed faces; by implication, this is considered the fastest growing face and therefore, the most attractive target for drug action. The (001) face of β-hematin was found to be highly corrugated, exposing aromatic surfaces as well as flexible propionic acid groups, vinyl and methyl groups in grooves which run parallel to the a-axis.[19] Using a *manual fitting* approach, the authors showed how the planar quinoline scaffold of inhibitors such as CQ and AQ could intercalate within these grooves between the upper and lower porphyrin rings, with additional close contacts between scaffold substituents and surface functional groups.[19] Inhibitors were considered in a monoprotonated state (i.e. side chain amine protonated and quinoline scaffold neutral), and the authors state that adsorption of these inhibitors would in fact not be possible if the quinoline N atom were protonated. CQ and AQ are, however, expected to accumulate in the DV as diprotic weak bases given the acidic pH (4.8–5.0).[20] In a related study, the differing activities of two diethylamino-alkoxyxanthone compounds, previously shown to form strong complexes with heme in solution,[16] were accounted for on the basis of their docking (adsorption) to the (001) and (011) faces.[15] More recently, L'abbate *et al.* have been able to rationalize (*post synthesis*) the structure-activity relationships for a series of 2-phenylbenzimidazole β-hematin inhibitors on the basis of their adsorption to the crystal surface.[21] In particular, the authors showed that the cumulative number of π-π interactions on the (001) and (011) faces was a predictor of activity.

In the current study, we demonstrate the first application of the *in silico* adsorption method from the ground up, in order to predict activity of new β-hematin inhibitors *prior to* their synthesis and evaluation. We describe structure-activity analyses for a set of eight clinically relevant antimalarial drugs that inhibit β-hematin formation, as well as a set of 53 cyclic scaffolds. Having identified primary and secondary binding sites on the (001) crystal face, we use the knowledge gained from the *in silico* study to guide the structure-based design and synthesis of five new amino-phenoxazine compounds with favourable adsorption energies and predicted β-hematin inhibitory activity. Since HZ remains an important antimalarial drug target, we anticipate that the findings of this study will be valuable to future rational design efforts. Importantly, the scaffold search provides a rationale for chemotypes that may be worthwhile pursuing in the development of new non-quinoline hemozoin-inhibiting antimalarials.

Results and Discussion

In silico adsorption of clinically relevant antimalarial drugs

Theoretical crystal morphology

Prior to performing the adsorption simulations, the external morphology of β-hematin was examined using BIOVIA MS Morphology (see **Table S1** for parameters).[22] The calculated attachment energies for the four faces that present in the external morphology of HZ crystals, namely the (100), (010), (011) and (001) faces, are reported (**Table S2**). Less negative values are associated with a greater morphological importance (overall size),[23] and thus the data predict that the crystals are dominated by the (100) and (010) faces, while the (011) and (001) faces are developed to a lesser extent (Figure 1, with further details in **Figure S1**). This theoretical external morphology is consistent with *in vivo* observations of native HZ extracted from *P. falciparum*.[6a] Attachment energy is also related to growth rate perpendicular to a particular face (i.e. the addition of the next layer) and thus the (001) face is predicted to be the fastest-growing.[23]

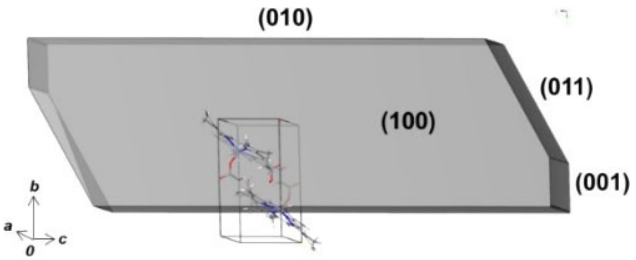

Figure 1. Theoretical morphology of a hemozoin/β-hematin crystal showing the four faces that dominate the external morphology. The unit cell used in the calculations is shown for reference.[24]

Adsorption of antimalarial drugs onto the β-hematin crystal faces

The molecular mechanics approach made use of the Adsorption Locator tool in BIOVIA Materials Studio (MS) to simulate the adsorption of inhibitors onto each of the four faces.[22] Following adsorption, each inhibitor was subjected to simulated annealing within the rigid binding site in order to optimize the fit. The *in silico* adsorption of CQ, AQ, QN, quinidine (QD), quinacrine (QC), PYR, halofantrine (Hf) and piperaquine (PPQ) (**Figure S2**) to the (001), (011), (010) and (100) faces of a β-hematin crystal was investigated. In cases where different protonation states of the drug were possible, only those that account for at least 5% of the total speciation at the pH of the DV (~4.8) were investigated (**Table S3**). The calculated adsorption energies are reported in **Table S4** and confirm that in general, adsorption to the (001) face is preferred. Absolute values are up to 1.3 times larger on the (001) face compared to the (011) and (010) faces, with only Hf showing a marginally weaker affinity (0.96 times) for the (001) face compared to the (011) face. Compared to the (100) face, absolute values for all species are 1.2 to 1.6 times larger on the (001) face. Following hierarchical ordering of the adsorption energies (**Table S5**), we found that compounds containing a bicyclic (quinoline) scaffold adsorb less favourably in general compared to compounds that contain a core scaffold of three rings. A point of departure in this regard is the *bis*-quinoline compound PPQ (specifically PPQ3+), which shows the most favourable adsorption of all the antimalarial drugs on average. Possible reasons for this are discussed below. Of the compounds containing tricyclic scaffolds, PYR performs better on average than either QC or Hf, which suggests that the functionalization on the PYR scaffold may be more favourable towards adsorption.

Given the preference of the antimalarial drugs to adsorb to the (001) face, we inspected the docking poses for possible trends in location(s) and orientation(s) on this particular face. As anticipated, the planar aromatic scaffold of each drug is observed to occupy the deep furrow that runs along the a-axis (**Figure S1c**), and which is cradled on the top and bottom by porphyrin (aromatic) systems. In further discussions, we refer to this location as the primary adsorption site (**Figure S1b**); it is contained within the boundaries of a single unit cell and periodicity in the [100] direction gives rise to adjacent primary adsorption sites. These could in theory be targeted by molecules that contain multiple, suitably-spaced adsorbing scaffolds. Prior to performing the adsorption calculations, we anticipated that PPQ may demonstrate this behaviour. However, we only ever observed adsorption *via* a single quinoline scaffold, which suggests that the flexible propyl linker is not sufficiently pre-organized to direct the second quinoline moiety into an adjacent primary adsorption site. Rather, the improved adsorption capabilities of PPQ are likely due to the increased degrees of freedom in the molecule that enable it to maximize interactions on the crystal surface outside of the primary adsorption site.

The adsorption of diprotic CQ (CQ2+) exemplifies the typical adsorption geometry found for the antimalarial drugs (Figure 2). The quinoline moiety occupies the primary adsorption site on the (001) face and is involved in π-π stacking interactions to the porphyrin moieties above and below (type 1 interaction), with interaction distances of 3.4–3.7 Å. The quinoline nitrogen atom, despite being protonated, points inwards and is involved in a close contact with a porphyrin vinyl group (type 2 interaction, (cyclic scaffold)NH^+···H(vinyl), 2.9 Å).

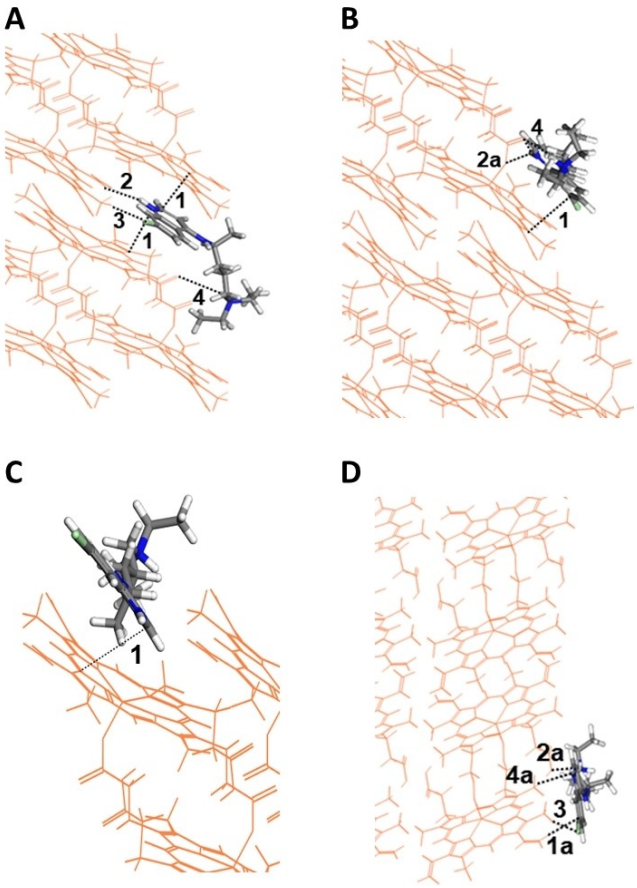

Figure 2. The adsorption of diprotic chloroquine (CQ2+) to the surface of β-hematin. **A** Adsorption to the (001) face: the quinoline moiety occupies the primary adsorption site within the furrow that runs along the *a*-axis, where π–π stacking interactions (type 1) ranging from 3.4–3.7 Å dominate the drug-target interaction. In addition, favourable interactions occur between the drug and crystal as follows: (cyclic scaffold)NH^+···H(vinyl), 2.9 Å (type 2); (cyclic scaffold)7Cl···H(methyl), 2.8 Å (type 3); and a weak hydrogen bond (side chain)NH···O=C(propionic acid), 4.0 Å (type 4). **B** Adsorption to the (011) face: the drug occupies the secondary adsorption site, where a single π-π stacking interaction (type 1) of 3.7 Å is observed. Two interactions involving the cyclic scaffold heteroatom are observed (type 4a); however, unlike on the (001) face, these occur to the coordinated propionate group: (cyclic scaffold)NH^+···O=C(propionate), 2.0 Å and (cyclic scaffold)NH^+···O-(propionate), 2.5 Å; a strong hydrogen bond (side chain)NH^+···O=C-(propionate), 2.2 Å (type 4) is also observed. **C** Adsorption to the (010) face: the drug occupies a shallow primary adsorption site, where a single π-π stacking interaction (type 1) of 4.0 Å is observed. **D** Adsorption to the molecularly-flat (100) face. While π-π stacking interactions are observed, these typically involve a porphyrin *vinyl substituent* and not the porphyrin *core* as on the (001) and (011) faces (type 1a). The 7-chloro and terminal amine heteroatoms are each involved in attractive interactions with a methyl group on the porphyrin periphery (type 3 and 5). In all cases, the β-hematin crystal is shown in orange, and the orientation thereof corresponds to **Figure S1** for clarity. Close contacts between CQ and the crystal are indicated as dashed black lines. See **Table S8a–d** for further details.

Consequently, the electronegative 7-chloro substituent is also directed inwards, where it is observed to form an attractive interaction with the H atom of a porphyrin methyl group, since the latter carries a partial positive charge (type 3 interaction, (cyclic scaffold)7Cl···H(methyl), 2.8 Å). The flexible N^1,N^1-diethylpentane-1,4-diamine side chain extends away from the primary adsorption site and interacts with the surface functional groups in what we define as a secondary adsorption site. In particular, owing to protonation, the terminal amine of CQ2+ forms a weak charge-assisted hydrogen bond with a surface-exposed propionic acid group (type 4 interaction, (side chain)NH···O=C(propionic acid), 4.0 Å, 104.6°). The adsorption location of CQ2+ in the current study is consistent with the prediction by Leiserowitz and co-workers;[19] however, differences in the distances for the close contacts discussed above were found (**Table S6**). This is not unexpected, however, since we used a molecular dynamics/simulated annealing approach in the current study compared to a *manual docking* approach in the previous study.[19] The authors also considered the docking of CQ1+ (terminal amine protonated but neutral quinoline N-atom), which is not likely to be present in the digestive vacuole.

The adsorption of all other antimalarial drugs (AQ, QN, QD, QC, PYR, Hf and PPQ) to the (001) face is similar to CQ2+, with the cyclic scaffold occupying the primary adsorption site in each case (**Table S7**). The observed close contacts are summarized in **Table S8a**. Type 1 (π-π stacking) interactions are observed for all dominant species at pH 4.8, with interaction distances ranging between 3.3–3.9 Å. Type 2 interactions are observed for all heterocyclic species, with the scaffold N-atom interacting with either a vinyl- or methyl-group on the porphyrin periphery. Given its hydrocarbon scaffold, Hf does not display type 2 interactions. Interactions involving scaffold substituents (type 3) are observed in all cases. Specifically, halogen atoms (if present) tend to form attractive interactions with vinyl- or methyl-groups; similar interactions involving the methoxy group were observed for three of the four drugs containing this substituent (QN, QD, and PYR, however, not QC). Finally, intermolecular hydrogen bonding between terminal amine functional groups and the porphyrin propionic acid carbonyl group (type 4) is observed for all drugs except QD and AQ. The distances vary from 2.1–3.9 Å, while the bond angle varies from 105° to 171°. In addition to these four common interaction types, QN, QD and Hf each feature a close contact involving their aryl methanol substituent (type 5). An additional intramolecular hydrogen bond (type 6) is observed in PYR between the scaffold N-atom and the terminal amine, and in AQ between the terminal amine and phenol groups in the side chain.

Compared to the (001) face, the terrain of the (011) and (010) faces is much flatter (**Figure S1**). A primary adsorption site is still present; however, it is less deep. A secondary adsorption site is also retained on the (011) face, and in general, the antimalarial drugs show a preference for adsorbing to the (011) face at this site. A consequence of this is that the number of π-stacking interactions is reduced in many cases from that seen on the (001) face, which could account for the lower adsorption energies observed for the (011) and (010) faces. In the case of CQ2+, π-π interactions (type 1) at lengths of 3.7 Å and 4.0 Å are observed on the (011) and (010) faces, respectively. The protonated quinoline nitrogen atom is involved in two hydrogen bonding interactions to the coordinated propionate group: (cyclic scaffold)NH^+···O=C(propionate), 2.0 Å, 160.1° (type 2a) and (cyclic scaffold)NH^+···O(propionate), 2.5 Å, 141.3° (type 2a). Finally, the protonated terminal amine in the side chain of CQ2+ forms a strong charge-assisted hydrogen bond with the coordinated propionate group: (side chain)NH^+···O=C-(propionate), 2.2 Å, 174.8° (type 4). The adsorption of all other antimalarial drugs (AQ, QN, QD, QC, PYR, Hf and PPQ) to the (011) and (010) faces is similar to CQ2+ (**Table S7**), where they form at least one π-π stacking interaction (type 1) at distances varying between 3.3 and 4.0 Å. The remaining close contacts formed on these two faces are summarized in **Table S8b** and **Table S8c**. In contrast to the (001), (011) and (010) faces, the (100) face is molecularly flat and there are no primary or secondary binding sites. As a consequence, the adsorption energies are considerably less, as reported above in **Table S4**. The adsorption of CQ2+ and the other antimalarial drugs (AQ, QN, QD, QC, PYR, Hf and PPQ) is shown in **Table S7**, and the close contacts are summarized in **Table S8d**. Apart from PYR, π-π stacking (type 1) interactions are observed for all of the antimalarial drugs. However, these occur between the drug scaffolds and a porphyrin *vinyl substituent* (rather than the porphyrin *core* as observed on the (001) and (011) faces). Porphyrin methyl groups frequently interact with heteroatoms on the drug scaffold or side chains (type 3 and type 5), while hydrogen bonding between the drugs and surface-exposed propionate/propionic acid groups is also observed (type 4).

Correlation between adsorption energies and β-hematin inhibitory activity

CQ, AQ and QN have been shown to inhibit HZ formation in the cell.[25] This mode of action has been inferred from β-hematin studies for the remaining five drugs,[26] although some inconsistencies are noted for acridine compounds such as QC.[27] All antimalarial drugs investigated in the *in silico* study were purchased and (re)tested for synthetic HZ (β-hematin) inhibitory activity using a biomimetic detergent (NP-40) assay,[28] the results of which are reported in **Table S9**. This was necessary as in the original descriptions of the assay, only the activities of CQ and AQ are reported. A strong correlation ($r^2 = 0.95$, $P = 0.0002$) is observed between the β-hematin IC_{50} values and the asexual antiplasmodium activity against the chloroquine-sensitive 3D7 strain (**Figure S3a**), which is consistent with previous studies.[27,29] We next investigated correlations between β-hematin IC_{50} values and adsorption energy values. The latter were weighted based on the fractional abundance (>5%) of different protic species at pH 4.8 (**Table S3**) and added together to obtain a single adsorption energy value for each drug (**Table S9**). Considering the average adsorption energy for each drug across the four faces, we found a good correlation ($r^2 = 0.72$, $P = 0.008$) with β-hematin inhibitory activity (Figure 3a). We then considered the individual faces in turn. It is noteworthy

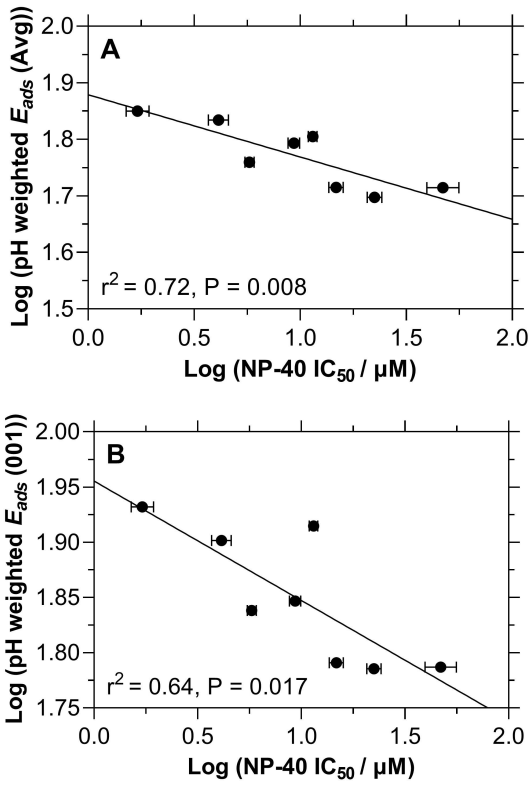

Figure 3. Relationship between *in silico* adsorption energy and β-hematin inhibitory activity. Linear correlations observed between the log of the β-hematin inhibitory activity determined using the NP-40 assay,[28] and **A** the log of the average adsorption energy to the (001), (011), (010) and (100) crystal faces (r^2 = 0.72, P = 0.008); **B** the log of the adsorption energy determined for the (001) crystal face (r^2 = 0.64, P = 0.017). The plotted data are reported in **Table S9**.

that the adsorption of antimalarial drugs to the (001) face gives a good correlation (r^2 = 0.64, P = 0.017) with β-hematin inhibitory activity that agrees with the correlation obtained using average values (Figure 3b). Significant correlations were also found between β-hematin inhibitory activity and the adsorption of antimalarial drugs to the (011), (010) and (100) faces (**Figure S3b–d**, respectively). The least favourable correlation is observed for the (011) face (r^2 = 0.53, P = 0.044), while an improvement was found on the (010) face (r^2 = 0.63, P = 0.019). The best correlation overall, albeit by a small margin, is observed for the (100) face (r^2 = 0.75, P = 0.005). The latter result is initially surprising given that this face is molecularly flat, however, it is possible that it is better able to accommodate the adsorption of inhibitors *via* formation of a greater number of non-specific van der Waals interactions. To our knowledge, the correlations reported here are the first to demonstrate a relationship between *in silico* adsorption energy and experimental β-hematin activity. While determined for a static system in the sense that the crystal was not growing, the data provide strong support for the hypothesized mechanism of inhibition of β-hematin formation *via* adsorption of inhibitors (as additives) to the crystal surface.

In silico prediction and design of new non-quinoline β-hematin inhibitors

Adsorption of cyclic scaffolds onto the crystal faces

Fifty-three scaffolds were considered, comprising 15 monocyclic, (**M1–M15**, **Table S10a**), 22 bicyclic (**B1–B22**, **Table S10b**) and 16 tricyclic (**T1–T16**, **Table S10c**) compounds. Generalized structures of these are shown in Figure 4. When different protonation states (>5%) at pH 4.8 were considered (**Table S11**), the scaffold count rose to 61 (16 monocyclic, 27 bicyclic and 18 tricyclic). Admittedly, this selection of heterocyclic and aromatic scaffolds is not exhaustive. Fragments that occur frequently in drug-like molecules were prioritized, with systematic variations in some cases (e.g. of the heteroatom) giving rise to additional scaffolds for consideration. Amongst the scaffolds investigated were the four occurring in the clinically relevant antimalarial drugs discussed above, namely quinoline (**B13**) present in CQ, AQ, QN, QD and PPQ, acridine (**T1**) present in QC, benzo[b][1,5]naphthyridine (**T3**) present in PYR, and phenanthrene (**T12**) present in Hf. Lumefantrine, an aryl methanol antimalarial related to Hf, contains the fluorene scaffold (**T13**), while the oldest synthetic antimalarial compound, methylene blue,[30] which is used today as a standard in gametocytocidal assays, contains the phenothiazine scaffold (**T10**).

The adsorption energy (E_{ads}) values for each scaffold on the different faces are reported in **Table S12**. When the average E_{ads} values were ranked from 1 to 61, the 18 tricyclic scaffolds were found to be the best adsorbers with the most negative adsorption energies, followed by the 27 bicyclic scaffolds, and thereafter the 16 monocyclic scaffolds (**Figure S4**). This pattern

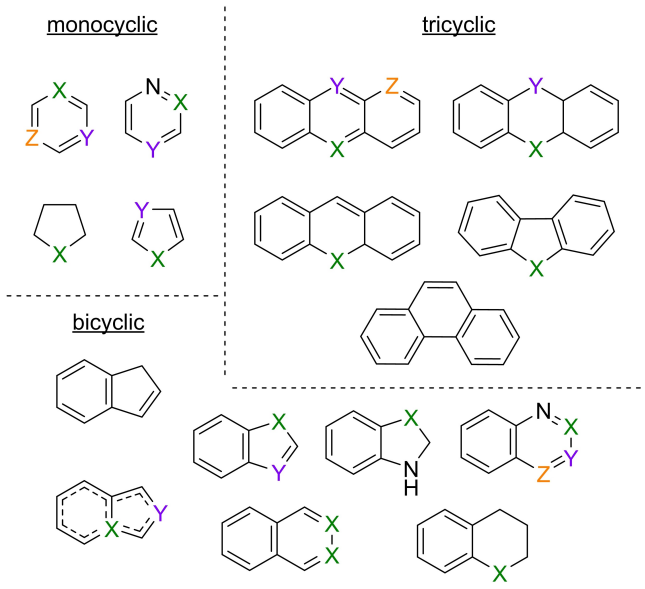

Figure 4. A total of 53 monocyclic, bicyclic and tricyclic scaffolds were adsorbed to the (001), (011), (010) and (100) faces of a β-hematin crystal. X, Y and Z indicate the positions of carbon, nitrogen, oxygen or sulphur atoms (see **Table S10** for further details).

is consistently observed on the (011), (010) and (100) faces with few exceptions. While this general trend is also observed to a large extent on the (001) face, there is a greater degree of overlap between the tricyclic and bicyclic scaffolds (Figure 5a). During the development of a lead compound, considering drug likeness, as well as ligand efficiency, are important factors.[31] The latter metric considers compound size (in terms of number of non-hydrogen atoms, N) in the form of a relative binding energy (in this case E_{ads}/N). The size-independent ligand efficiency (SILE=E_{ads}/$N^{0.3}$) is an improved metric when considering molecules of varying sizes, such as the different cyclic scaffolds in this study,[32] and is reported for each scaffold in **Table S12**. A statistically-significant positive correlation (r^2 = 0.49, $P < 0.0001$) is observed between absolute SILE values and number of non-hydrogen atoms (Figure 5b). Compounds with the least favourable SILE values (ranked 57–61) on each face (and on average) include pyrrolidine (**M7**), tetrahydrofuran (**M8**), tetrahydrothiophene (**M9**), pyrrole (**M10**) and imidazole (**M13**). This is almost certainly due to their small size, which limits the number of interactions with the crystal surface. Interestingly, these and other monocyclic scaffolds occur frequently as fragments in larger lead compounds (for example benzamides,[33] triarylimidazoles,[34] and others[35]) that display both β-hematin inhibition and antiplasmodium activity. This suggests that despite their individual limitations, the cumulative effect of multiple monocyclic scaffolds may still afford good adsorption properties.

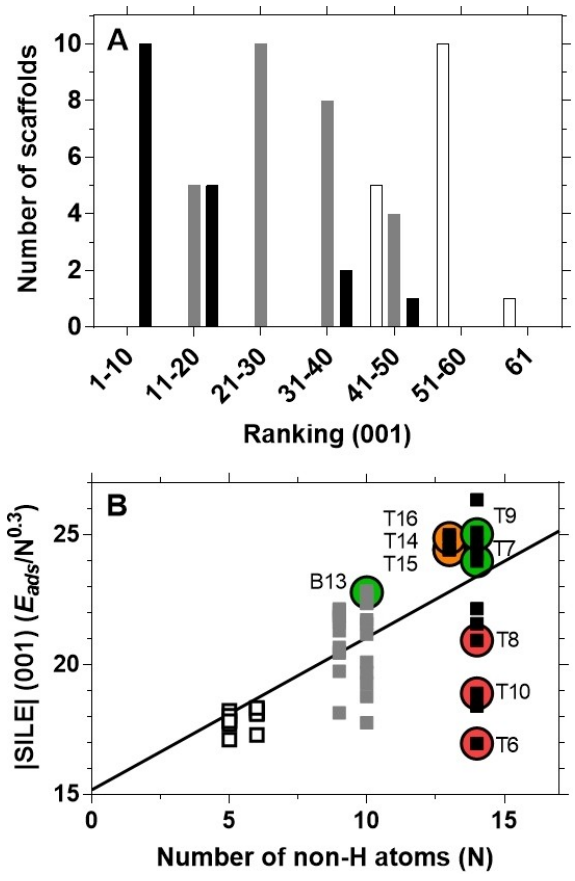

Figure 5. Adsorption of cyclic scaffolds to the (001) face of β-hematin. **A** Ranking of adsorption energies (E_{ads}/kcal.mol^{-1}) determined for 61 scaffolds (including neutral and protonated forms) on the (001) face. **B** Plot of absolute SILE values for the (001) face vs the number of non-hydrogen atoms in the 61 monocyclic, bicyclic and tricyclic scaffolds (r^2 = 0.49, $P < 0.0001$). Quinoline (**B13**), 4aH-xanthene (**T7**) and phenoxazine (**T9**) appear above the trendline (green circles), as do dibenzothiophene (**T16**), carbazole (**T14**), and dibenzofuran (**T15**) (orange circles). On the contrary, the sulphur-containing tricyclic scaffolds **T6**, **T8** and **T10** (red circles) have very weak affinity for the (001) face. General colour code in both cases: monocyclic (white), bicyclic (grey) and tricyclic (black) scaffolds. In total, 16 monocyclic, 27 bicyclic and 18 tricyclic scaffolds were considered.

Of the bicyclic scaffolds investigated, the quinoline scaffold (**B13**) is of most interest given its incorporation into several clinically-relevant antimalarial drugs, as well as those shown to inhibit hemozoin in the cell (CQ, AQ, QN).[25] Considering the SILE values, the neutral and monoprotic forms of **B13** are ranked between 17th–24th on the (011), (010) and (100) faces. Interestingly, both forms of **B13** fare marginally better on the (001) face, where they are ranked in positions 14 and 15, respectively. Consequently, **B13** falls above the correlation line in Figure 5b, suggesting that it may be a privileged scaffold with respect to adsorption to the (001) face. By contrast, the top ten adsorbing scaffolds (irrespective of face) are all tricyclic in structure. This is consistent with the observations above for antimalarial drugs, where compounds with tricyclic scaffolds were better able to adsorb compared to bicyclic species. This is purportedly due to their extended aromatic scaffolds, which facilitate docking into the primary adsorption site on the (001) and (011) faces. In the case of the fastest-growing (001) face, five of the top ten adsorbing scaffolds are present in clinically-relevant antimalarial drugs, namely benzo[b][1,5]naphthyridine (**T3**, 1st), phenanthrene (**T12**, 2nd), fluorene (**T13**, 4th) and acridine (**T1**, 6th and **T1(1+)**, 10th). Anthracene (**T11**), the all-carbon analogue of **T1**, ranked 7th, while dibenzothiophene (**T16**), carbazole (**T14**), and dibenzofuran (**T15**), the S-, N-, and O-analogues of **T13**, are ranked 5th, 8th, and 9th respectively. Phenoxazine (**T9**), the O-analogue of phenothiazine (**T10**) that is present in methylene blue, ranked 3rd. This scaffold also appears above the trend line in Figure 5b, suggesting it may have similarly favourable adsorption properties to quinoline (**B13**). The **T1** and **T3** scaffolds rank frequently in the top ten on the (011), (010) and (100) faces, as do **T7** (apart from the (001) face) and **T9**. A notable exception to this trend is the tricyclic scaffold **T6**, which is ranked in 58th place on the (001) face when considering SILE values. Related sulphur-containing tricyclic scaffolds (**T8** and **T10**) also perform poorly on this face (in positions 32 and 40, respectively), and are seen as outliers in Figure 5b. Notably, Bayesian models for β-hematin inhibition and antiplasmodium activity found fingerprints containing sulphur to be unfavourable.[36]

Taken together, our *in silico* results indicate that the heteroatom analogues of fluorene (**T14–T16**), as well as the related 4aH-xanthene (**T7**) and phenoxazine (**T9**) scaffolds, may be worthwhile pursuits in the development of new antimalarials that specifically target hemozoin/β-hematin inhibition. They all show excellent adsorption capabilities (Figure 5b), are non-quinoline and importantly, these chemotypes have not been used to date in antimalarial chemotherapy. It is noteworthy that

the oxidized form of phenoxazine (**T9**), phenoxazinium, is present in a number of dyes such as basic blue and brilliant cresyl blue. These and other experimental π-delocalized lipophilic cations are thought to accumulate in plasma and mitochondrial membranes.[37] Akin to methylene blue, these compounds exhibit potent antimalarial activity against CQ resistant *P. falciparum* strains; an EC_{50} of 2.8 nM against the K1 strain and IC_{50} values <10 nM against both D6 and W2 strains, have been reported for basic blue and brilliant cresyl blue, respectively.[37–38] Derivatization of the phenoxazinium scaffold has led to the discovery of active compounds with a tetracyclic benzo[*a*]phenoxazine scaffold.[39] Lead compound SSJ-183 was reported with an IC_{50} of 7.6 nM against the K1 strain and selectivity index of ~7300 when tested on L6 myoblast cells.[39a] A follow-up study showed that this compound inhibited growth of all stages, but affected ring-stage parasites in particular at low concentration.[40] More recently, a series of acylphenoxazine compounds with low cytotoxicity against HEK293T and HepG2 cells, but potent selectivity for *Plasmodium* strains has been reported.[41] While the literature certainly points to the antimalarial potential of phenoxazine derivatives, this scaffold has not been considered specifically with respect to HZ inhibition. Thus given its highest overall ranking (3rd place) for a non-antimalarial scaffold with respect to adsorption to the crystal surface, phenoxazine (**T9**) was our scaffold of choice moving forward to experimentally validate the adsorption hypothesis.

Design and synthesis of new amino-phenoxazine compounds

Owing to cross-resistance between a number of clinically-relevant drugs, in particular those containing a quinoline nucleus,[42] chemical diversity is of uttermost importance in the development of new antimalarial compounds. The phenoxazine scaffold identified by the *in silico* scaffold search reported above, is not a structural motif that currently features in any clinically relevant antimalarial drugs and therefore has potential to address the necessity for chemical variance. On its own, this heterocyclic scaffold may afford π-stacking (type 1) and scaffold N-atom (type 2) interactions, which we have shown to be important for adsorption within the primary binding site on the β-hematin crystal surface. To access hydrogen bonding (type 4) interactions between the test compound(s) and the crystal surface, a side chain containing an amine functional group is essential. Owing to its relative simplicity, as well as availability of relevant starting materials, we initially considered the N^1,N^1-diethylpentane-1,4-diamine side chain present in both CQ and QC. Given that our focus was primarily on the design and synthesis of proof-of-concept compounds to test the adsorption hypothesis, we excluded other scaffold substituents (e.g. halogens) as a means of simplifying the synthetic strategy. Mono-substitution of the phenoxazine scaffold with an amine side chain could lead to a mixture of four regioisomers, thus we first assessed each with respect to adsorption capabilities using our *in silico* approach. The adsorption energies for the four phenoxazine (P) regioisomers suggest that isomer **P2a**, with the CQ side chain (indicated by "a") in the 2-position, would adsorb most favourably (Table 1).

Of the remaining regioisomers, which showed no statistical difference in E_{ads} values, **P3a** was also included in our target library given that it is structurally related to the 3-substituted phenoxazinium and phenothiazinium scaffolds in brilliant cresyl blue and methylene blue, respectively. Finally, to diversify our small proof-of-concept library, we considered two additional amine side chain variants, giving rise to a total of five derivatives (Figure 6). The *in silico* adsorption energies of all target compounds to the (001) crystal face are reported in Table 2.

Chemistry

Very few literature examples exist for the synthesis of the amino-phenoxazine compounds of interest (Figure 6). One reported strategy involved a reductive amination approach,[43] which was deemed unsuitable as a general approach for our targets, since the required carbonyl sidechains would be more difficult to obtain, or in the case of the phenyl group (**P2c**), impossible with this strategy. A more modern and appropriate approach envisaged either an Ullmann or Buchwald-Hartwig aryl amination strategy (Scheme 1).[44] Furthermore, both the acetyl 2-bromophenoxazine **1**[45] and 3-bromophenoxazine **2**[46] required for this strategy have also been previously reported.

Table 1. Calculated adsorption energies for regioisomers with the CQ side chain to the (001) face of β-hematin.

Compound	E_{ads} [kcal.mol^{-1}]
P1a	-67.6 ± 0.1
P2a	-74.0 ± 0.2
P3a	-69.5 ± 0.8
P4a	-71.6 ± 0.1

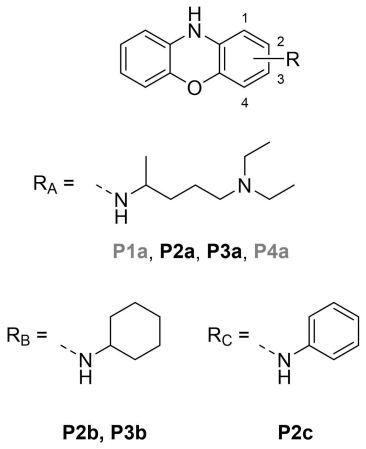

Figure 6. Proof-of-concept amino-phenoxazine compounds with predicted β-hematin inhibitory activity. Compound codes are delineated as follows: P = phenoxazine core; number 1–4 = position of side chain; a/b/c = different side chains (i.e. R_A, $-R_B$, $-R_C$). Compounds indicated in black were synthesized for further evaluation, while those indicated in grey were only considered for *in silico* studies.

Table 2. *In silico* adsorption energies and experimental activity data determined for proof-of-concept amino-phenoxazine β-hematin inhibitors.

Compound	E_{ads} (001) [kcal.mol^{-1}]	NP-40 IC_{50} [μM]	3D7 IC_{50} [μM]	Late-stage gametocyte [μM][b]
P2a	−74.0 ± 0.2	4.7 ± 0.6	0.64 ± 0.05	–
P2b	−62.4 ± 0.1	7.0 ± 1.0	5.2 ± 0.4	> 10
P2c	−58.2 ± 0.1	80 ± 3.0	9.0 ± 1.0	~ 10
P3b[a]	−59.0 ± 0.6	*40 ± 3.0*	*2.0 ± 0.6*	*1.07 ± 0.06*
P3a′[a]	−66.9 ± 0.6	*260 ± 30*	–	*1.60 ± 0.09*
CQ	−61.8 ± 0.2	15 ± 1.0	0.029	–

[a] 3-Substituted phenoxazine compounds could not be synthesized with unambiguous certainty or purity, and therefore the activity data, while insightful, is considered tentative. [b] Methylene blue and MMV048 controls showed 94.8 and 96.0% inhibition, respectively, at 5 μM. (–) Value not determined in this study. E_{ads} and NP-40 measurements were repeated in triplicate, with standard deviation and SEM values reported, respectively. Three independent measurements, each repeated in technical triplicate, were carried out for 3D7 and late-stage gametocyte assays. In both cases, errors reported are SEM.

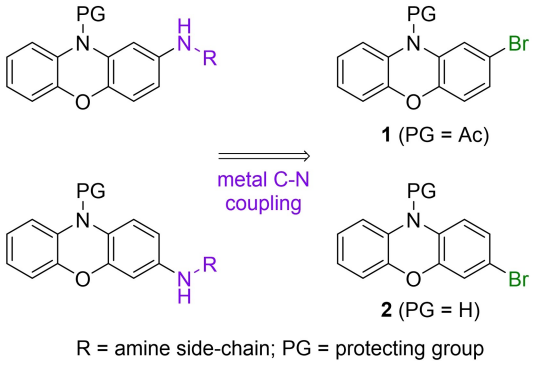

Scheme 1. General disconnection strategy envisaged for generating the proof-of-concept amino-phenoxazine compounds.

The required brominated phenoxazines were obtained after various optimisations and minor changes to the published syntheses (see Supporting Information for details).[45–47] We noted at this point that these compounds, particularly the unprotected phenoxazines, were very sensitive to light and rapidly degraded unless kept in the dark. The amination reactions were perniciously capricious and required a significant number of optimisation studies to find reaction conditions that worked (see Scheme 2 and Supporting Information for full details). The 2-substituted amino-phenoxazines **P2a–c** could be isolated as their hydrochloride salts, after hydrolysis of the acetyl on the phenoxazine nitrogen atom under acidic conditions (see Experimental Section for yields). The structure of **P2b·HCl** was confirmed by single crystal X-ray diffraction (**Figure S5**). It should be noted that the hydrochloride salts significantly improved their stability, otherwise impurities rapidly formed. The main impurity for the 2-substituted phenoxazines **P2a–c** appeared to be a covalent dimer that was detected by HRMS. In the case of cyclohexyl phenoxazine **P2b**, the structure of the dimer was also confirmed using single crystal X-ray diffraction (**Figure S5**).

The attempted synthesis of the 3-substituted amino-phenoxazines **P3a–b** was, however, much more challenging. The aryl amination reactions were successful; however, removal of the Boc-protecting group, whilst facile, always returned highly unstable compounds. **P3a** was found to rapidly oxidise to **P3a′** (Scheme 2), as inferred from HRMS data and analogous known structures such as brilliant cresyl blue. Attempts to isolate the product as a more stable salt (phosphate or chloride) also yielded the oxidized form. Consequently, acquiring a good ^{1}H NMR spectrum was near impossible; in the case of the phosphate salt, it was found to be extremely hygroscopic, and

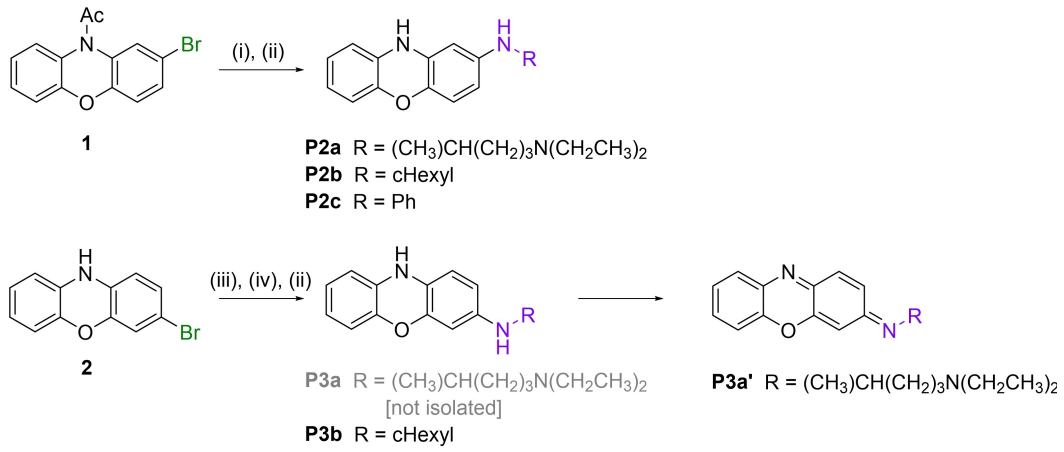

Scheme 2. General scheme for the aryl amination reactions. Reagents and conditions: (i) R-NH_2, CuI, L-proline, DMSO, 40–60 °C, 1–7 d; (ii) HCl, EtOH, 90 °C, 20 min; (iii) Boc_2O, Et_3N, DMAP, DCM, rt, 4 h;(iv) R-NH_2, $Pd(OAc)_2$, Xantphos, $CsCO_3$, 1,4-dioxane, 90 °C.

the excess water dominated the spectrum (see Supporting Information). The hydrochloride salt on the other hand appeared to aggregate in all NMR solvents such that only broad indistinct signals could be measured. Compound **P3b** was found to be slightly more forgiving in that it did not rapidly oxidize, but again it was impossible to obtain an acceptable ^{1}H NMR spectrum since significant line broadening was observed. The overall result was that the 3-substituted phenoxazine compounds could not be synthesized with unambiguous certainty or purity. Whilst this was unfortunate, the 2-substituted phenoxazines remained the primary focus of the study with respect to our hypothesis that adsorption energy could serve as a predictor of β-hematin inhibitory activity. Nevertheless, preliminary activity studies were also carried out for the 3-phenoxazine samples where possible.

Activity studies

β-Hematin and asexual blood stage activity

As described above for the antimalarial drugs, the five final compounds were evaluated for β-hematin inhibitory activity using a biomimetic NP-40 detergent assay.[28] **P2a** and **P2b** show low micromolar activity (IC_{50} = 4.7 ± 0.6 and 7.0 ± 1.0, respectively) that is comparable to AQ, while **P2c** shows 10-fold weaker β-hematin inhibitory activity (Table 2). Inclusion of these three new amino-phenoxazine hits strengthens the correlation found above for antimalarial drugs between the pH-weighted adsorption energy on the (001) face and β-hematin inhibitory activity (Figure 7). Of the 3-substituted amino-phenoxazines, an IC_{50} value of 40 μM was found for a freshly-prepared sample of **P3b**. We consider this value tentative, however, owing to its moderate instability and lack of unequivocal purity as indicated earlier. On the other hand, compound **P3a'** yielded an IC_{50} value > 100 μM and is considered inactive. Active compounds were further evaluated for antiplasmodium activity against the asexual blood stage of the *P. falciparum* 3D7 strain (Table 2). **P2a** showed the most promising blood stage activity, with an IC_{50} value of 0.64 ± 0.05 μM. While seven times less active than CQ, this sub-micromolar value is quite remarkable for a compound comprising only an unsubstituted scaffold and amine side chain.

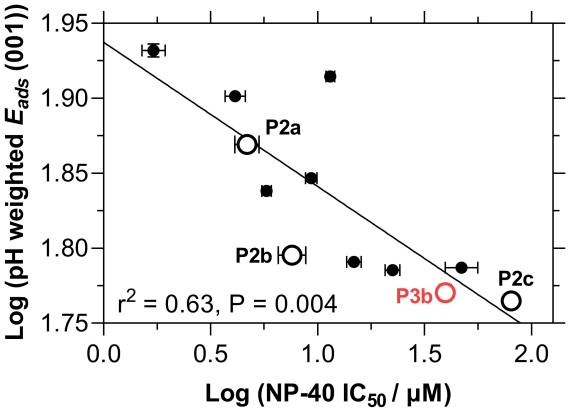

Figure 7. Relationship between *in silico* adsorption energy and β-hematin inhibitory activity. Linear correlation observed between the log of the β-hematin inhibitory activity determined using the NP-40 assay,[28] and log of the adsorption energy to the (001) crystal face (r^2 = 0.63, P = 0.004). The data are reported in Table 2. Antimalarial drugs are indicated as solid black circles, while four new amino-phenoxazine compounds are indicated as open circles. The data point for **P3b** (red) is tentative and not included in the correlation.

Late-stage gametocyte activity

Compounds **P2b**, **P2c**, **P3b** and **P3a'** were investigated for gametocytocidal activity. Sufficient amounts of **P2a** were unfortunately not available, although the 2-substituted amino phenoxazines were primarily of interest for their β-hematin inhibition, rather than gametocytocidal potential. The luciferase reporter assay platform using the NF54-Mal8p1.16-GFP-Luc reporter line was employed.[48] The hydrochloride salts of compounds **P2b** and **P2c** were inactive against late-stage *P. falciparum* gametocytes, even at 10 μM. This is consistent with the inactivity of CQ against late-stage gametocytes, and supports HZ formation as a primary target in the asexual blood stage.[49] For the remaining two compounds, dose-response curves could be obtained and moderate IC_{50} values of 1.1 ± 0.1 and 1.6 ± 0.1 μM for **P3b** and **P3a'**, respectively, were found. In light of compound instability, further experimental validation of these preliminary results is necessary before any potential polypharmacology (activity against multiple stages or multiple targets) is considered for the amino-phenoxazine compounds. The gametocyte activity data are reported in Table 2.

Conclusion

Efforts to introduce new hit compounds into the antimalarial drug development pipeline are especially important given that resistance continues to threaten the efficacy of clinically-relevant treatments. The heme detoxification pathway, in particular HZ formation, remains an important target for a number of these drugs. Together with eight clinically-relevant antimalarial drugs, we have shown that there is a statistically-significant correlation between experimental β-hematin inhibitory activity under biomimetic conditions and adsorption of new amine-phenoxazine inhibitors to the crystal surface, in particular the (001) face. Despite approximating the dynamic process of inhibition of β-hematin crystal growth using a rigid crystal structure, valuable insights have been gained that are expected to benefit future rational design efforts of new, non-quinoline β-hematin inhibitors. The studies of both the antimalarial drugs and the diverse scaffolds validate the important role of π-π stacking interactions in facilitating interaction between the drug/drug candidate and the crystal surface. Herein we have thus demonstrated the first (to our knowledge) use of an *in silico* method to predict β-hematin inhibitory activity based on adsorption energy *prior to* synthesis of a series of proof-of-concept amino-phenoxazine compounds.

Coupled with its promising β-hematin inhibitory activity, **P2a** in particular provides strong support for the adsorption hypothesis. Furthermore, the observed structure-activity relationship points to a synergism between inhibitor constituents (scaffold, substituents, and side chains) that underpins β-hematin inhibitory activity; at the same time, the substituents and side chains may be derivatized further to improve drug-likeness, in particular the solubility, of otherwise predominantly hydrophobic scaffolds. Therefore, the *in silico* method presented herein provides a readily-accessible tool by which to design and test various combinations of scaffold and substituents to maximize interactions with the β-hematin crystal surface. In the pursuit of new antimalarial hemozoin inhibitors, we expect that this may greatly reduce time misspent on inactive compounds.

Experimental Section

***In silico* adsorption studies**. All simulations were performed using the BIOVIA MS software package.[22] Firstly, the external habit of β-hematin crystals was investigated using the Morphology tool; specifically, we used the Bravais-Friedel Donnay-Harker (BFDH) method.[50] For a series of planes, their calculated attachment energies and respective growth rates facilitate morphology prediction using a Wulff plot.[51] The settings and parameters used are given in **Table S1**. Thereafter, the adsorption behavior of eight antimalarial drugs and 53 cyclic scaffolds (reported in **Figure S2** and **Table S10**, respectively) to the (001), (011), (010) and (100) crystal faces was investigated. The method has been described previously,[21] where the *in silico* approach was used *post-synthesis* to rationalize the β-hematin inhibitory activity of a series of 2-phenylbenzimidazole compounds. As before, calculations in the current study were performed for neutral and relevant protonated forms of all scaffolds.

Compounds. For general experimental details and details regarding synthesis of bromophenoxazines **1** and **2**, and 3-substituted phenoxazines **P3a**–**b** see Supporting Information.

1-(2-((5-(diethylamino)pentan-2-yl)amino)-10*H*-phenoxazin-10-yl)ethan-1-one (*N*-Ac-P2a). 2-bromo-phenoxazine **1** (0.748 g, 2.46 mmol, 1.00 eq.), N^1,N^1-diethylpentane-1,4-diamine (1.43 mL, 7.38 mmol, 3.00 eq.), *L*-proline (0.113 g, 0.984 mmol, 0.400 eq.) and DMSO (7.5 mL) were added to a Schlenk tube and degassed using the freeze-pump-thaw method. An argon atmosphere was established for the addition of copper(I) iodide (0.937 g, 4.92 mmol, 2.00 eq.), and the reaction mixture heated to 60 °C and stirred for 7 days. The reaction mixture was then quenched with a saturated NH_4Cl solution (10 mL) and diluted with DCM (10 mL). This was then extracted into DCM (3×20 mL), and the organic layers washed with H_2O (3×20 mL). The organic layer was then dried with $MgSO_4$, filtered and concentrated on the rotary evaporator. The product was purified by column chromatography (MeOH\DCM 1:10), producing a clear oil with a mass of 0.582 g with a yield of 62%. **IR (ATR, cm^{-1})**: 3310 (N–H), 2962 and 2644 (C–H), 1670 (C=O), 1479 (C=C), 756 (C–H). **^{1}H NMR (600 MHz, $CDCl_3$)** δ 7.37 (d, $^3J_{HH}$ = 7.7 Hz, 1H, Ar*H*), 7.15–7.11 (m, 1H, Ar*H*), 7.06–7.02 (m, 2H, Ar*H*), 6.88 (d, $^3J_{HH}$ = 8.8 Hz, 1H, Ar*H*), 6.76 (d, $^4J_{HH}$ = 2.4 Hz, 1H, Ar*H*), 6.42 (dd, $^3J_{HH}$ = 8.8 Hz, $^4J_{HH}$ = 2.6 Hz, 1H, Ar*H*), 3.44–3.37 (m, 1H, C*H*(CH_3)CH_2), 2.98 (q, $^3J_{HH}$ = 7.2 Hz, 4H, N(CH_2CH_3)$_2$), 2.88 (dt, $^3J_{HH}$ = 9.2, $^4J_{HH}$ = 6.4 Hz, 2H, $CH_2CH_2CH_2$), 2.29 (s, 3H, C(O)CH_3), 1.91–1.79 (m, 2H, $CH_2CH_2CH_2$), 1.65–1.51 (m, 2H, $CH_2CH_2CH_2$), 1.26 (t, $^3J_{HH}$ = 7.2 Hz, 6H, N(CH_2CH_3)$_2$), 1.15 (d, $^3J_{HH}$ = 6.3 Hz, 3H, CH(CH_3)CH_2).**^{13}C NMR (151 MHz, $CDCl_3$)*** δ 169.4, 151.7, 143.8, 142.6, 130.2, 129.5, 126.8, 125.1, 122.9, 117.1, 116.8, 111.8, 109.9, 51.7, 48.9, 46.6, 33.8, 23.3, 20.94, 20.89, 9.1 **HRMS(ESI$^+$)** calculated for $C_{23}H_{32}N_3O_2$: 382.2495, found $[M+H]^+$ 382.2504.

N^1,N^1-diethyl-N^4-(10*H*-phenoxazin-2-yl)pentane-1,4-diamine (P2a). Acetyl protected phenoxazine ***N*-Ac-P2a** (151 mg, 0.396 mmol, 1.00 eq.) was added to a degassed 0.265 M HCl ethanol solution (4.45 mL, 1.18 mmol, 3.00 eq.), and heated to 40 °C for 3 hours. The reaction was neutralized with 2 M NaOH, monitored by pH paper, and extracted into DCM (3×20 mL). The organic layer was then dried with $MgSO_4$, filtered and concentrated on the rotary evaporator. The product was purified by column chromatography (MeOH\DCM 1:10), producing a clear oil with a mass of 92.3 mg in a yield of 62%. **IR (ATR, cm^{-1})**: 3364 (N–H), 1639 and 1493 (C=C).**^{1}H NMR (400 MHz, $CDCl_3$)** δ 6.73–6.67 (m, 1H, Ar*H*), 6.64 (d, $^3J_{HH}$ = 3.9 Hz, 2H, Ar*H*), 6.51 (d, $^3J_{HH}$ = 8.5 Hz, 1H, Ar*H*), 6.39 (d, $^3J_{HH}$ = 7.7 Hz, 1H, Ar*H*), 5.89 (dd, $^3J_{HH}$ = 8.5 Hz, $^4J_{HH}$ = 2.5 Hz, 1H, Ar*H*), 5.73 (d, $^4J_{HH}$ = 2.5 Hz, 1H, Ar*H*), 5.19 (s, 1H, N*H*), 3.32 (m, 1H, C*H*(CH_3)CH_2), 2.60 (q, $^3J_{HH}$ = 7.3 Hz, 4H, N(CH_2CH_3)$_2$), 2.48 (m, 2H, $CH_2CH_2CH_2$), 1.61–1.38 (m, 4H, $CH_2CH_2CH_2$), 1.15 (d, $^3J_{HH}$ = 6.3 Hz, 3H, CH(CH_3)CH_2), 1.06 (t, $^3J_{HH}$ = 7.3 Hz, 6H, N(CH_2CH_3)$_2$). **^{13}C NMR (101 MHz, $CDCl_3$)** δ 144.4, 144.2, 135.2, 132.1, 131.5, 123.1, 121.4, 116.4, 115.7, 113.5, 105.6, 99.2, 53.1, 49.2, 46.9, 35.2, 23.9, 21.0, 11.7. **HRMS–Positive**: *m/z* $[M+H]^+$ calculated for $C_{21}H_{30}N_3O$: 340.2389, found: 340.2385.

1-(2-(cyclohexylamino)-10*H*-phenoxazin-10-yl)ethan-1-one (*N*-Ac-P2b). The same coupling and work-up protocol for ***N*-Ac-P2a** was followed. 2-Bromophenoxazine **1** (1.00 g, 3.29 mmol, 1.00 eq.), cyclohexylamine (1.13 mL, 9.87 mmol, 3 eq.), *L*-proline (152 mg, 1.32 mmol, 0.400 eq.), copper(I)iodide (126 mg, 0.658 mmol, 0.200 eq.) and DMSO (3.30 mL). The reaction was stirred for 72 hours at a temperature of 60 °C. After work-up, the product was purified by column chromatography (EtOAc\Hexane 1:5), producing the product as a clear oil with a mass of 541 mg in a yield of 51%. **IR (ATR, cm^{-1})**: 3380 (N–H), 2926 and 2848 (C–H), 1664 (C=O), 1481 (C=C), 802 (C–H). **^{1}H NMR (600 MHz, $CDCl_3$)** δ 7.46 (dd, $^3J_{HH}$ = 8.2 Hz, $^3J_{HH}$ = 1.0 Hz, 1H, Ar*H*), 7.18–7.14 (m, 1H, Ar*H*), 7.10–7.06 (m, 2H, Ar*H*), 6.92 (d, $^3J_{HH}$ = 8.7 Hz, 1H, Ar*H*), 6.71 (d, $^4J_{HH}$ = 2.4 Hz, 1H, Ar*H*), 6.41 (dd, $^3J_{HH}$ = 8.7, $^4J_{HH}$ = 2.4 Hz, 1H, ArH_1), 3.47 (br s, 1H, N*H*), 3.19 (tt, $^3J_{HH(aa)}$ = 10.1 Hz, $^3J_{HH(ae)}$ = 3.7 Hz, 1H, $H_{(cyclohexyl)}$), 2.33 (s, 3H, CO_2CH_3), 2.04 (dd, $^3J_{HH(aa)}$ = 12.8 Hz, $^3J_{HH(ae)}$ = 3.1 Hz, 2H, $H_{cyclohexyl}$), 1.78–1.72 (m, 2H, $H_{cyclohexyl}$), 1.68–1.62 (m, 1H, $H_{cyclohexyl}$), 1.41–1.32 (m, 2H, $H_{cyclohexyl}$), 1.27–1.18 (m, 1H, $H_{cyclohexyl}$), 1.18–1.10 (m, 2H, $H_{cyclohexyl}$). **^{13}C NMR (151 MHz, $CDCl_3$)** δ 169.4, 151.8, 143.8, 142.6, 130.4, 129.6, 126.8, 125.3, 122.9, 117.2, 116.9, 111.7, 109.7, 52.4, 33.5, 26.0, 25.1, 23.4. **HRMS–Positive**: *m/z* $[M+H]^+$ calculated for $C_{20}H_{23}N_2O_2$: 323.1760, found: 323.1765.

***N*-cyclohexyl-10*H*-phenoxazin-2-amine (P2b)**. The same hydrolysis and work-up protocol for **P2a** was followed. Actyl-2-cyclohexylamino phenoxazine ***N*-Ac-P2b** (598 mg, 1.97 mmol, 1.00 eq.) was heated under reflux for 4 h. The product was allowed to crystallize for 7 days, producing clear rectangular crystals with a mass of 218 mg in a yield of 35%. **MP**: 228–230 °C (decomposed). **IR (ATR, cm^{-1})**: 3248 (N–H), 2766 and 2651 (C–H), 1493 (C=C), 732 (C–H). [NMR assignments made using 2D NMR spectra, see Supporting Information for details] **^{1}H NMR (600 MHz, DMSO-*d*)** δ ppm 10.93 (br s, 2H, NH_{15}), 8.70 (s, 1H, NH_{10}), 6.74 (ddd, $^3J_{HH}$ = 7.7 Hz, $^3J_{HH}$ = 7.0 Hz, $^4J_{HH}$ = 2.0 Hz, 1H, ArH_3), 6.68 (d, $^3J_{HH}$ = 8.3 Hz, 1H, Ar$H_{11\ or\ 12}$), 6.66–6.55 (m, 4H, ArH_1, ArH_2, Ar$H_{11\ or\ 12}$, ArH_{14}), 6.49 (dd, $^3J_{HH}$ = 7.7, $^4J_{HH}$ = 1.2 Hz, 1H, ArH_6), 3.18 (m, 1H, $H_{16(cyclohexyl)}$), 1.94 (d, $^3J_{HH(aa)}$ = 12.6 Hz, 2H, $H_{17(cyclohexyl)}$ or $H_{21(cyclohexyl)}$), 1.74 (d, $^3J_{HH(aa)}$ = 13.3 Hz, 2H, $H_{18(cyclohexyl)}$ and $H_{20(cyclohexyl)}$), 1.58 (d, $^3J_{HH(aa)}$ = 12.6 Hz, 1H, $H_{19(cyclohexyl)}$), 1.41 (qd, $^3J_{HH(aa)}$ = 12.2 Hz, $^3J_{HH(ae\ or\ ee)}$ = 3.32 Hz, 2H, $H_{18(cyclohexyl)}$ and $H_{20(cyclohexyl)}$), 1.21 (td, $^3J_{HH(aa)}$ = 12.6 Hz, $^3J_{HH(ae\ or\ ee)}$ = 3.3 Hz, 2H, $H_{17(cyclohexyl)}$ and $H_{21(cyclohexyl)}$), 1.10 (tt, $^3J_{HH(aa)}$ = 12.6 Hz, $^3J_{HH(ae)}$ = 3.3 Hz, 1H, $H_{19(cyclohexyl)}$). **^{13}C (151 MHz, DMSO-*d*)** δ ppm 142.5 (ArC_5), 141.8 (ArC_{13}), 133.4 (ArC_8), 131.4 (ArC_4), 130.7 (ArC_9), 124.1 (ArC_3), 120.8 (ArC_1), 115.5 (Ar$C_{11\ or\ 12}$), 115.1 (ArC_2), 114.3 (Ar$C_{11\ or\ 12}$), 113.5 (ArC_6),

107.3 (ArC_{14}), 59.4 (ArC_{16}), 28.8 (Ar$C_{17\ or\ 21,\ and\ 18\ or\ 20}$), 24.8 (Ar$C_{19}$), 23.9 (Ar$C_{17\ or\ 21,\ and\ 18\ or\ 20}$). **HRMS-Positive**: *m/z* $[M+H]^+$ calculated for $C_{18}H_{21}N_2O$: 281.1654; found: 281.1659.

1-(2-(phenylamino)-10*H*-phenoxazin-10-yl)ethan-1-one (*N*-Ac-P2c). The same coupling and work-up protocol for ***N*-Ac-P2a** was followed. 2-bromophenoxazine **1** (1.00 g, 3.28 mmol, 1.00 eq.), aniline (1.50 mL, 16.4 mmol, 5.00 eq.), *L*-proline (755 mg, 6.56 mmol, 2.00 eq.), copper(I)iodide (625 mg, 3.28 mmol, 1.00 eq.) and DMSO (10 mL). The reaction was stirred for 72 hours at a temperature of 60 °C. The product was purified by column chromatography (EtoAc \Hexane 1:5), isolating a white solid with a mass of 502 mg at a yield of 48%. **IR (ATR, cm^{-1})**: 3343 (N–H),1659 (C=O), 1479 and 1264 (C=C), 736 (C–H). **^{1}H NMR (400 MHz, $CDCl_3$)** δ 7.43 (dd, $J=8.3$, 1.4 Hz, 1H, Ar*H*), 7.29–7.21 (m, 3H, Ar*H*), 7.21–7.17 (m, 1H, Ar*H*), 7.15–7.09 (m, 2H, Ar*H*), 7.05–6.99 (m, 3H, Ar*H*), 6.92 (ddd, $J=8.3$, 4.8, 1.4 Hz, 2H, Ar*H*), 5.66 (s, 1H, N*H*), 2.33 (s, 3H, CO_2CH_3). **^{13}C NMR (101 MHz, $CDCl_3$)** δ 169.3, 151.5, 145.8, 143.7, 138.9, 130.3, 129.6, 129.5, 127.1, 125.2, 123.3, 121.0, 117.5, 117.3, 117.2, 117.0, 116.0, 23.3. **HRMS–Positive**: *m/z* $[M+H]^+$ calculated for $C_{20}H_{17}N_2O_2$: 317.1290; found: 317.1298.

***N*-phenyl-10*H*-phenoxazin-2-amine (P2c)**. The same hydrolysis protocol for **P2a** was followed. Acetyl-2-phenylamino phenoxazine ***N*-Ac-P2c** (598 mg, 1.97 mmol, 1.00 eq.) was heated under reflux for 4 h. The reaction mixture was neutralized with 2 M NaOH, (monitored with pH paper) and the product extracted into EtOAc (approximately 3×10 mL per 10 mg product). Purification was achieved via column chromatography (EtOAc\Hexane 1:5), and the product isolated as 135 mg of a white solid in a yield of 25%. **IR (ATR, cm^{-1})**: 3366 (N–H), 1595 and 1499 (C=C), 740 (C–H). **^{1}H NMR (400 MHz, $CDCl_3$)** δ 7.26–7.20 (m, 2H, Ar*H*), 6.96 (dt, $^3J_{HH}=8.4$ Hz, $^4J_{HH}=1.1$ Hz, 2H, Ar*H*), 6.88 (dd, $^3J_{HH}=7.4$ Hz, $^4J_{HH}=1.1$ Hz, 1H, Ar*H*), 6.76–6.67 (m, 1H, Ar*H*), 6.67–6.66 (m, 2H, Ar*H*), 6.60 (d, $^3J_{HH}=8.4$ Hz, 1H, Ar*H*), 6.40–6.34 (m, 2H, Ar*H*), 6.20 (d, $^4J_{HH}=2.5$ Hz, 1H, Ar*H*), 5.41 (s, 1H,N*H*), 5.10 (s, 1H, N*H*). **^{13}C NMR (101 MHz, $CDCl_3$)** δ 144.1, 143.9, 139.0, 138.6, 132.2, 131.2, 129.5, 123.5, 121.7, 120.5, 117.2, 116.4, 115.9, 113.5, 112.0, 104.9. **HRMS–Positive**: *m/z* $[M+H]^+$ calculated for $C_{18}H_{15}N_2O$: 275.1184, found: 275.1171.

***tert*-butyl 3-bromo-10*H*-phenoxazine-10-carboxylate**. 3-Bromo phenoxazine (200 mg, 0.763 mmol, 1.00 eq.) was added to an oven-dried round-bottom flask, thereafter an argon atmosphere was established, and the sample dissolved in DCM (2 mL). A solution consisting of DCM (2 mL), Boc_2O (0.259 mL, 1.14 mmol, 1.50 eq.), triethylamine (0.212 mL, 1.52 mmol, 2.00 eq.) and DMAP (9.3 mg, 0.076 mmol, 0.10 eq.) was subsequently added. The reaction was stirred at room temperature for 4 hours. Upon completion the reaction mixture was diluted with DCM (10 mL), washed with H_2O (3×30 mL), dried with $MgSO_4$, filtered and the solvent reduced on a rotary evaporator. The product was purified via column chromatography (EtOAc\Hexane 1:20), producing 275 mg of a white solid with a yield of 99%. **IR (ATR, cm^{-1})**: 2970 (C–H), 1711 (C=O), 1481 (C=C), 748 (C–H). **^{1}H NMR (400 MHz, $CDCl_3$)** δ 7.53–7.49 (m, 1H, Ar*H*), 7.39 (dd, $^3J_{HH}=8.3$ Hz, $^4J_{HH=}0.6$ Hz, 1H, Ar*H*), 7.21–7.17 (m, 2H, Ar*H*), 7.10 (m, 2H, Ar*H*), 7.04–7.01 (m, 1H, Ar*H*), 1.54 (s, 9H, CH(CH_3)). **^{13}C NMR (101 MHz, $CDCl_3$)** δ 151.8, 151.2, 150.1, 128.7, 128.3, 126.32, 126.28, 126.2, 125.2, 123.5, 119.9, 118.5, 116.7, 83.1, 28.3. **HRMS–Positive**: *m/z* $[M-C(CH_3)_3+H]^+$ calculated for $C_{13}H_9NO_3Br$: 305.9766, found: 305.9769.

***tert*-butyl 3-([5-(diethylamino)pentan-2-yl]amino)-10*H*-phenoxazine-10-carboxylate (*N*-Boc-P3a)**. 1,4-Dioxane (2.3 mL), N^1,N^1-diethylpentane-1,4-diamine (0.442 mL, 2.28 mmol, 2.00 eq.), Cs_2CO_3 (743 mg, 2.28 mmol, 2.00 eq.), Xantphos (81.0 mg, 0.137 mmol, 0.120 eq.) and Boc-3-bromo phenoxazine **2** (414 mg, 1.14 mmol, 1.00 eq.) were added to an oven-dried Schlenk flask which was covered in tinfoil. The reaction mixture was then degassed in triplicate using the freeze-pump-thaw method and back-filled with argon. Lastly, $Pd(OAc)_2$ (25.6 mg, 0.114 mmol, 0.100 eq) was added to the reaction mixture and the argon atmosphere was re-established. The reaction was stirred at 90 °C for 7 days. The reaction was then quenched with H_2O (10 mL) and diluted with EtOAc (30 mL) and separated. The organic layer was washed with H_2O (3×30 mL), dried with $MgSO_4$, filtered and reduced on a rotary evaporator. The product was purified via column chromatography (MeOH\DCM 1:20), producing 325 mg of a clear oil with a yield of 65%. **^{1}H NMR (400 MHz, $CDCl_3$)** δ 7.50 (dd, $^3J_{HH}=7.7$ Hz, $^4J_{HH}=1.6$ Hz, 1H, Ar*H*), 7.29–7.23 (m, 1H, Ar*H*), 7.11–6.96 (m, 3H, Ar*H*), 6.27 (dd,$^3J_{HH}=6.7$, $^4J_{HH}=2.4$ Hz, 2H, Ar*H*), 3.68 (br s, 1H, NH), 3.47–3.34 (m, 1H, ($CH(CH_3)CH_2$), 2.53 (q, $^3J_{HH}=7.1$ Hz, 4H, $N(CH_2CH_3)_2$), 2.46–2.39 (m, 2H, $CH_2CH_2CH_2$), 1.52 (m, 13H, $CH(CH_3)$ and $CH_2CH_2CH_2$), 1.17 (d, $^3J_{HH}=6.2$ Hz, 3H, $(CH(CH_3)CH_2)$, 1.02 (t, $^3J_{HH}=7.1$ Hz, 6H, $N(CH_2CH_3)_2$).**^{13}C NMR (101 MHz, $CDCl_3$)** δ 152.5, 151.4, 150.4, 146.3, 129.5, 125.64, 125.58, 125.2, 122.8, 118.2, 116.5, 108.2, 100.2, 82.0, 52.9, 48.7, 46.8, 35.0, 28.3, 23.6, 20.8, 11.5. **HRMS–Positive**: *m/z* $[M+H]^+$ calculated for $C_{26}H_{38}N_3O_3$: 440.2913; found: (M+H) 440.2915.

***tert*-butyl 3-(cyclohexylamino)-10*H*-phenoxazine-10-carboxylate (*N*-Boc-P3b)**. Distilled dioxane (0.3 mL), cyclohexylamine (32 µl, 0.276 mmol, 2.00 eq.), Cs_2CO_3 (90 mg, 0.276 mmol, 2.00 eq.), Xantphos (9.6 mg, 0.017 mmol, 0.12 eq.) and *tert*-butyl 3-bromo-10*H*-phenoxazine-10-carboxylate (50 mg, 0.138 mmol, 1.00 eq.) were added to an oven-dried Schlenk flask which was covered in tinfoil. The reaction mixture was degassed in triplicate using the freeze-pump-thaw method and back-filled with argon. Lastly, $Pd(OAc)_2$ (3.1 mg, 0.014 mmol, 0.100 eq) was added and the argon atmosphere re-established. The reaction was stirred at 90 °C for 72 hours. The reaction was then quenched with H_2O (10 mL) and diluted with EtOAc (30 mL) and separated. The organic layer was washed with H_2O (30 mL × 3) and subsequently dried with $MgSO_4$, filtered and reduced on a rotary evaporator. The product was purified via column chromatography (MeOH\DCM 1:20) producing a clear oil, with a mass of 12.1 mg with a yield of 23%. **IR (ATR, cm^{-1})**: 3386 (N–H), 2972 and 2854 (C–H), 1706 (C=O), 1486 (C=C), 1248 (C–N), 751 (C–H). **^{1}H NMR (400 MHz, $CDCl_3$)** δ 7.50 (dd, $^3J_{HH}=7.7$, $^4J_{HH}=1.8$ Hz, 1H, Ar*H*), 7.26 (d, $^3J_{HH}=9.4$ Hz, 1H, Ar*H*), 7.10–6.99 (m, 3H, Ar*H*), 6.28 (dd, $^3J_{HH}=6.8$, $^4J_{HH}=2.5$ Hz, 2H, Ar*H*), 3.54 (br s, 1H, N*H*), 3.23–3.15 (m, 1H, $CH_{(cyclohexyl)}$), 2.10–2.00 (m, 2H, $H_{(cyclohexyl)}$), 1.80–1.71 (m, 2H, $H_{(cyclohexyl)}$), 1.65 (m, 1H, $H_{(cyclohexyl)}$), 1.52 (s, 9H, OCH(CH_3)), 1.42–1.30 (m, 2H, $H_{(cyclohexyl)}$), 1.27–1.21 (m, 1H, $H_{(cyclohexyl)}$), 1.13 (m 2H, $H_{(cyclohexyl)}$). **^{13}C NMR (101 MHz, $CDCl_3$)** δ 152.5, 151.5, 150.5, 146.0, 129.6, 125.73, 125.67, 125.3, 122.9, 118.3, 116.5, 108.4, 100.3, 82.1, 52.1, 33.5, 28.4, 26.0, 25.1. **HRMS–Positive**: *m/z* $[M+H]^+$ calculated for $C_{23}H_{29}N_2O_3$: 381.2178; found: (M+H) 381.2184.

Activity studies. *β-hematin inhibition.* This was determined in a Nonidet P-40 (NP-40) detergent system according to a previously reported method in 96-well plates.[28] IC_{50} values were determined from triplicate measurements, together with the standard error of the mean (SEM).

Antiplasmodium activity. This was determined as described before with minor modifications.[52] Briefly, *P. falciparum* parasites (3D7 strain) were cultured at 2–3% parasitemia in A^+ erythrocytes (4% hematocrit) in RPMI-1640 GlutaMAX™ media with 25 mM HEPES, 11 mM glucose, 200 µM hypoxanthine (dissolved in 0.5 M NaOH), 24 µg/mL gentamycin and 0.6% (m/v) Albumax-II. Blood was obtained from the Western Cape Blood Bank (WCBS) in Cape Town. Ethics exemption (HREC reference number X19/03/005) was obtained for testing inhibitors on *P. falciparum* parasite cultures grown in human blood as culture medium. Drug assays were set up on synchronized asexual ring-stage parasites. In each instance, assays were set up using a 1% parasitaemia and a 1% haematocrit suspension in the presence of different concentrations of the compounds tested. Parasites were grown for 96 h in a gas

controlled incubator (93% N_2, 3% O_2, and 4% CO_2) at 37 °C. CQ was used as the positive drug control at 1 μM. No drug was used for the negative drug control, which allowed the parasites to proliferate in an unrestricted manner. After 96 h the parasites were lysed in lysis solution containing 20 mM Tris-HCl (pH 7.5), 5 mM EDTA, 0.008% w/v saponin, 0.08% v/v Triton X-100 containing SYBR™ Gold DNA stain (Invitrogen, ThermoFisher Scientific Inc., Bremen, Germany). Fluorescence was measured using a TECAN Spark® multimode microplate reader (Tecan Trading AG, Switzerland) and the data analysis was done using SigmaPlot, version 12 (Systat Software Inc., Chicago, IL, USA). Percentage parasite proliferation was plotted against the logarithm of compound concentration, and curve fitting was performed by nonlinear regression (typically using the equation $y = a/(1 + (x/IC_{50})^b)$ to yield the compound concentration required for 50% inhibition (IC_{50} values). IC_{50} values determined were from three biological repeats ($n = 3$), each determined in triplicate. The error indicated in the IC_{50} values represents the standard error of the mean (SEM).

Gametocyte activity. Gametocytes were produced as per Reader *et al.*[49,53] from *P. falciparum* NF54-Mal8p1.16-GFP-Luc,[48] and each batch validated for viability and functionality before use. All *in vitro* experiments involving human blood donors and human malaria parasites hold ethics approval from the University of Pretoria Research Health Sciences Ethics Committee (506/2018) and Natural and Agricultural Sciences Ethics Committee (NAS 180000094). This work abides by the Declaration of Helsinki principles. Drug assays were set up on day 10 (representing >90% stage IV/V gametocytes). Assays were set up using a 2–3% gametocytemia, 1.5% hematocrit culture and 48 h drug pressure under hypoxic conditions (90% N_2, 5% O_2, and 5% CO_2) at 37 °C, stationary. Luciferase activity was determined in 30 μL parasite lysates by adding 30 μL luciferin substrate (Promega Luciferase Assay System) at room temperature and detection of resultant bioluminescence at an integration constant of 10 s with the GloMax®-Multi+ Detection System with Instinct® Software. Methylene blue (5 μM) and an internal compound (MMV390048, 5 μM) are routinely included as controls. Data for IC_{50} values are from three independent biological repeats, performed in technical triplicates.

Crystallography. Single-crystal X-ray intensity data were collected on a Bruker 4 axis KAPPA D8 Venture X-ray diffractometer equipped with an INCOATEC IμS 3.0 microfocus sealed tube (MoKα radiation λ = 0.71073 Å) fitted with multilayer mirror optics monochromator. Data were captured with a PHOTON II CPAD detector. Data collection was carried out at 100 K using an Oxford Cryosystems cryostat (800 series Cryostream Plus) attached to the diffractometer. Data collection and reduction were carried out using the Bruker software package APEX3,[54] using standard procedures. All structures were solved and refined using SHELX-2016[55] employed within the X-Seed environment.[56] Hydrogen atoms were placed in calculated positions using riding models. Diagrams were generated using POV-Ray.[57]

CCDC deposition numbers: 2155681 (for **P2b**.HCl), 2155683 (for covalent dimer of **P2b**), 2155682 (for Boc-**2**), 2155684 (for **P3b**.HCl).

Acknowledgements

*We gratefully acknowledge Dr S. C. Pelly (ex. Department of Chemistry and Polymer Science, Stellenbosch University), Dr W. J. Gerber and B. P. Greyling (Department of Chemistry and Polymer Science, Stellenbosch University) for assistance with Materials Studio software installation and license management; the Centre for High Performance Computing (CHPC) for use of their resources and access to Materials Studio license; Prof D. A. Haynes (Department of Chemistry and Polymer Science, Stellenbosch University) for assistance with solution of the single-crystal X-ray diffraction structure of **P2b** dimer. The research reported in this publication was supported by the National Institute of Allergy and Infectious Diseases of the National Institutes of Health (NIH) under Award R01AI110329 and the National Research Foundation (NRF) of South Africa to K.d.V. (UID 87962) and to LMB (UID84627 and UID110666). T.O. acknowledges the NIH and NRF for bursary support. The content is solely the responsibility of the authors and does not necessarily represent the official views of the NIH or NRF.*

Conflict of Interest

The authors declare no conflict of interest.

Data Availability Statement

The data that support the findings of this study are available in the supplementary material of this article.

Keywords: adsorption · crystal growth · β-hematin · heterocycles · inhibitors · phenoxazines · pi interactions

[1] P. Alonso, A. M. Noor, *Lancet* **2017**, *390*, 2532–2534.
[2] *World Malaria Report 2021*, World Health Organization, **2021**. (https://www.who.int/teams/global-malaria-programme/reports/world-malaria-report-2021).
[3] a) T. J. Egan, *Targets* **2003**, *2*, 115–124; b) S. Kapishnikov, D. Grolimund, G. Schneider, E. Pereiro, J. G. McNally, J. Als-Nielsen, L. Leiserowitz, *Sci. Rep.* **2017**, *7*, 7610.
[4] a) M. F. Oliveira, J. C. P. d'Avila, C. R. Torres, P. L. Oliveira, A. J. Tempone, F. D. Rumjanek, C. M. S. Braga, J. R. Silva, M. Dansa-Petretski, M. A. Oliveira, W. De Souza, S. T. Ferreira, *Mol. Biochem. Parasitol.* **2000**, *111*, 217–221; b) M. F. Oliveira, J. R. Silva, M. Dansa-Petretski, W. de Souza, C. M. S. Braga, H. Masuda, P. L. Oliveira, *FEBS Lett.* **2000**, *477*, 95–98; c) T. J. Egan, J. M. Combrink, J. Egan, G. R. Hearne, H. M. Marques, S. Ntenteni, B. T. Sewell, P. J. Smith, D. Taylor, D. A. van Schalkwyk, J. C. Walden, *Biochem. J.* **2002**, *365*, 343–347.
[5] a) A. V. Pandey, V. K. Babbarwal, J. N. Okoyeh, R. M. Joshi, S. K. Puri, R. L. Singh, V. S. Chauhan, *Biochem. Biophys. Res. Commun.* **2003**, *308*, 736–743; b) V. Papalexis, M.-A. Siomos, N. Campanale, X.-G. Guo, G. Kocak, M. Foley, L. Tilley, *Mol. Biochem. Parasitol.* **2001**, *115*, 77–86; c) D. J. J. Sullivan, I. Y. Gluzman, D. E. Goldberg, *Science* **1996**, *271*, 219–222; d) D. Jani, R. Nagarkatti, W. Beatty, R. Angel, C. Slebodnick, J. Andersen, S. Kumar, D. Rathore, *PLoS Pathog.* **2008**, *4*, e1000053.
[6] a) T. J. Egan, J. Y.-J. Chen, K. A. de Villiers, T. E. Mabotha, K. J. Naidoo, K. K. Ncokazi, S. J. Langford, D. McNaughton, S. Pandiancherri, B. R. Wood, *FEBS Lett.* **2006**, *580*, 5105–5110; b) J. M. Pisciotta, I. Coppens, A. K. Tripathi, P. F. Scholl, J. Shuman, S. Bajad, V. Shulaev, D. J. Sullivan Jr., *Biochem. J.* **2007**, *402*, 197–204; c) A. N. Hoang, K. K. Ncokazi, K. A. de Villiers, D. W. Wright, T. J. Egan, *Dalton Trans.* **2010**, *39*, 1235–1244; d) A. N. Hoang, R. D. Sandlin, A. Omar, T. J. Egan, D. W. Wright, *Biochemistry* **2010**, *49*, 10107–10116.
[7] D. Kuter, R. Mohunlal, S.-M. Fitzroy, C. Asher, P. J. Smith, T. J. Egan, K. A. de Villiers, *CrystEngComm* **2016**, *18*, 5177–5187.
[8] K. A. de Villiers, M. Osipova, T. E. Mabotha, I. Solomonov, Y. Feldman, K. Kjaer, I. Weissbuch, T. J. Egan, L. Leiserowitz, *Cryst. Growth Des.* **2009**, *9*, 626–632.
[9] S. Kapishnikov, A. Weiner, E. Shimoni, G. Schneider, M. Elbaum, L. Leiserowitz, *Langmuir* **2013**, *29*, 14595–14602.
[10] J. M. Combrinck, K. Y. Fong, L. Gibhard, P. J. Smith, D. W. Wright, T. J. Egan, *Malar. J.* **2015**, *14*, 1–14.

[11] R. Openshaw, K. Maepa, S. J. Benjamin, L. Wainright, J. M. Combrinck, R. Hunter, T. J. Egan, *ACS Infect. Dis.* **2021**, *7*, 362–376.
[12] K. A. de Villiers, T. J. Egan, *Acc. Chem. Res.* **2021**, *54*, 2649–2659.
[13] J. Gildenhuys, T. le Roex, T. J. Egan, K. A. de Villiers, *J. Am. Chem. Soc.* **2013**, *135*, 1037–1047.
[14] S.-M. Fitzroy, J. Gildenhuys, T. Olivier, N. O. Tshililo, D. Kuter, K. A. de Villiers, *Langmuir* **2017**, *33*, 7529–7537.
[15] I. Solomonov, M. Osipova, Y. Feldman, C. Baehtz, K. Kjaer, I. K. Robinson, G. T. Webster, D. McNaughton, B. R. Wood, I. Weissbuch, L. Leiserowitz, *J. Am. Chem. Soc.* **2007**, *129*, 2615–2627.
[16] M. K. Riscoe, J. X. Kelly, R. Winter, *Curr. Med. Chem.* **2005**, *12*, 2539–2549.
[17] K. N. Olafson, M. A. Ketchum, J. D. Rimer, P. G. Vekilov, *Proc. Nat. Acad. Sci.* **2015**, *112*, 4946–4951.
[18] K. N. Olafson, T. Q. Nguyen, J. D. Rimer, P. G. Vekilov, *Proc. Nat. Acad. Sci.* **2017**, *114*, 7531–7536.
[19] R. Buller, M. L. Peterson, Ö. Almarsson, L. Leiserowitz, *Cryst. Growth Des.* **2002**, *2*, 553–562.
[20] R. Hayward, K. J. Saliba, K. Kirk, *J. Cell Sci.* **2006**, *119*, 1016–1025.
[21] F. P. L'abbate, R. Muller, R. Openshaw, J. M. Combrinck, K. A. de Villiers, R. Hunter, T. J. Egan, *Eur. J. Med. Chem.* **2018**, *159*, 243–254.
[22] BIOVIA, 6.0 ed., Dassault Systèmes BIOVIA, San Diego.
[23] P. Hartman, P. Bennema, *J. Cryst. Growth* **1980**, *49*, 145–156.
[24] S. Pagola, P. W. Stephens, D. S. Bohle, A. D. Kosar, S. K. Madsen, *Nature* **2000**, *404*, 307–310.
[25] J. M. Combrinck, T. E. Mabotha, K. K. Ncokazi, M. A. Ambele, D. Taylor, P. J. Smith, H. C. Hoppe, T. J. Egan, *ACS Chem. Biol.* **2013**, *8*, 133–137.
[26] A. Dorn, S. R. Vippagunta, H. Matile, C. Jaquet, J. L. Vennerstrom, R. G. Ridley, *Biochem. Pharmacol.* **1998**, *55*, 727–736.
[27] D. N. H. Tam, G. M. Tawfik, A. E. El-Qushayri, G. M. Mehyar, S. Istanbuly, S. Karimzadeh, V. L. Tu, R. Tiwari, T. Van Dat, P. T. V. Nguyen, K. Hirayama, N. T. Huy, *Malar. J.* **2020**, *19*, 298.
[28] a) M. D. Carter, V. V. Phelan, R. D. Sandlin, B. O. Bachmann, D. W. Wright, *Comb. Chem. High Throughput Screening* **2010**, *13*, 285–292; b) R. D. Sandlin, M. D. Carter, P. J. Lee, J. M. Auschwitz, S. E. Leed, J. D. Johnson, D. W. Wright, *Antimicrob. Agents Chemother.* **2011**, *55*, 3363–3369.
[29] S. R. Hawley, P. G. Bray, M. Mungthin, J. D. Atkinson, P. M. O'Neill, S. A. Ward, *Antimicrob. Agents Chemother.* **1998**, *42*, 682–686.
[30] G. Lu, M. Nagbanshi, N. Goldau, M. Mendes Jorge, P. Meissner, A. Jahn, F. P. Mockenhaupt, O. Muller, *BMC Med.* **2018**, *16*, 59.
[31] K. E. Hevener, R. Pesavento, J. Ren, H. Lee, K. Ratia, M. E. Johnson, *Meth. Enzymol.* **2018**, *610*, 265–309.
[32] J. W. M. Nissink, *J. Chem. Inf. Model.* **2009**, *49*, 1617–1622.
[33] K. J. Wicht, J. M. Combrinck, P. J. Smith, R. Hunter, T. J. Egan, *J. Med. Chem.* **2016**, *59*, 6512–6530.
[34] a) K. J. Wicht, J. M. Combrinck, P. J. Smith, R. Hunter, T. J. Egan, *ACS Med. Chem. Lett.* **2017**, *8*, 201–205; b) C. G. L. Veale, J. Jayram, S. Naidoo, D. Laming, T. Swart, T. Olivier, M. P. Akerman, K. A. de Villiers, H. C. Hoppe, V. Jeena, *RSC Med. Chem.* **2020**, *11*, 85–91.
[35] R. D. Sandlin, K. Y. Fong, K. J. Wicht, H. M. Carrell, T. J. Egan, D. W. Wright, *Int. J. Parasitol.* **2014**, *4*, 316–325.
[36] K. J. Wicht, J. M. Combrinck, P. J. Smith, T. J. Egan, *Bioorg. Med. Chem.* **2015**, *23*, 5210–5217.
[37] K. Takasu, *Chem. Pharm. Bull.* **2016**, *64*, 656–667.
[38] J. L. Vennerstrom, M. T. Makler, C. K. Angerhofer, J. A. Williams, *Antimicrob. Agents Chemother.* **1995**, *39*, 2671–2677.
[39] a) J.-F. Ge, C. Arai, M. Yang, A. Bakar Md, J. Lu, N. S. M. Ismail, S. Wittlin, M. Kaiser, R. Brun, S. A. Charman, T. Nguyen, J. Morizzi, I. Itoh, M. Ihara, *Med. Chem.* **2010**, *1*, 360–364; b) X. L. Shi, J. F. Ge, B. Q. Liu, M. Kaiser, S. Wittlin, R. Brun, M. Ihara, *Bioorg. Med. Chem. Lett.* **2011**, *21*, 5804–5807.
[40] S. Schleiferbock, C. Scheurer, M. Ihara, I. Itoh, I. Bathurst, J. N. Burrows, P. Fantauzzi, J. Lotharius, S. A. Charman, J. Morizzi, D. M. Shackleford, K. L. White, R. Brun, S. Wittlin, *Drug Des. Dev. Ther.* **2013**, *7*, 1377–1384.
[41] T. Tougan, K. Takahashi, M. Ikegami-Kawai, M. Horiuchi, S. Mori, M. Hosoi, T. Horii, M. Ihara, M. Tsubuki, *Malar. J.* **2019**, *18*, 237.
[42] B. Blasco, D. Leroy, D. A. Fidock, *Nat. Med.* **2017**, *23*, 917–928.
[43] A. K. Sparkes, (Universal Oil Products Company, Delaware, USA), US Pat. No. 3413291A, **1968**.
[44] P. A. Forero-Cortés, A. M. Haydl, *Org. Process Res. Dev.* **2019**, *23*, 1478–1483.
[45] I. Thomé, C. Bolm, *Org. Lett.* **2012**, *14*, 1892–1895.
[46] a) M. Jahanfar, K. Suwa, K. Tsuchiya, K. O. Ogino, *Open J. Org. Polym. Mater.* **2013**, *03*, 46–52; b) S. Yamamoto, D. Goto, T. Sagisaka, M. Shinoda, M. Inoue, F. Kaneko, T. Yashiro, (Ricoh Company, Ltd., Japan), US Pat. No. 10935862-B2, **2020**.
[47] a) Y. Kanazawa, T. Yokota, H. Ogasa, H. Watanabe, T. Hanakawa, S. Soga, M. Kawatsura, *Tetrahedron* **2015**, *71*, 1395–1402; b) A. B. Gamble, J. Garner, C. P. Gordon, S. M. J. O'Conner, P. A. Keller, *Synth. Commun.* **2007**, *37*, 2777–2786; c) C. Deldaele, G. Evano, *ChemCatChem* **2016**, *8*, 1319–1328.
[48] S. H. Adjalley, G. L. Johnston, T. Li, R. T. Eastman, E. H. Ekland, A. G. Eappen, A. Richman, B. K. L. Sim, M. C. S. Lee, S. L. Hoffman, D. A. Fidock, *Proc. Nat. Acad. Sci.* **2011**, *108*, E1214–E1223.
[49] J. Reader, M. Botha, A. Theron, S. B. Lauterbach, C. Rossouw, D. Engelbrecht, M. Wepener, A. Smit, D. Leroy, D. Mancama, T. L. Coetzer, L. M. Birkholtz, *Malar. J.* **2015**, *14*, 213.
[50] J. D. H. Donnay, D. Harker, *Am. Mineral.* **1937**, *22*, 446–467.
[51] G. Wulff, *Z. Kristallogr. Mineral.* **1901**, *34*, 449–530.
[52] C. Spry, L. Barnard, M. Kok, A. K. Powell, D. Mahesh, E. T. Tjhin, K. J. Saliba, E. Strauss, M. de Villiers, *ACS Infect. Dis.* **2020**, *6*, 1844–1854.
[53] J. Reader, M. E. van der Watt, D. Taylor, C. Le Manach, N. Mittal, S. Ottilie, A. Theron, P. Moyo, E. Erlank, L. Nardini, N. Venter, S. Lauterbach, B. Bezuidenhout, A. Horatscheck, A. van Heerden, N. J. Spillman, A. N. Cowell, J. Connacher, D. Opperman, L. M. Orchard, M. Llinas, E. S. Istvan, D. E. Goldberg, G. A. Boyle, D. Calvo, D. Mancama, T. L. Coetzer, E. A. Winzeler, J. Duffy, L. L. Koekemoer, G. Basarab, K. Chibale, L. M. Birkholtz, *Nat. Commun.* **2021**, *12*, 269.
[54] Bruker, Bruker AXS Inc., Madison, Wisconsin, USA, **2016**.
[55] G. M. Sheldrick, *Acta Crystallogr.* **2008**, *A64*, 112–122.
[56] L. J. Barbour, *J. Appl. Crystallogr.* **2020**, *53*, 1141–1146.
[57] POV-Ray, Persistence of Vision Raytracer Pty. Ltd., **2003–2008**.

Manuscript received: March 16, 2022
Revised manuscript received: April 5, 2022
Accepted manuscript online: April 6, 2022
Version of record online: April 26, 2022